Multichannel Selective Femtosecond Coherent Control Based on Symmetry Properties

Zohar Amitay,* Andrey Gandman, Lev Chuntonov, and Leonid Rybak
Schulich Faculty of Chemistry, Technion-Israel Institute of Technology, Haifa 32000, Israel
(Received 30 September 2007; published 16 May 2008)

We present and implement a new scheme for extended multichannel selective femtosecond coherent control based on symmetry properties of the excitation channels. Here, an atomic nonresonant two-photon absorption channel is coherently incorporated in a resonance-mediated (2+1) three-photon absorption channel. By proper pulse shaping, utilizing the invariance of the two-photon absorption to specific phase transformations of the pulse, the three-photon absorption is tuned independently over an order-of-magnitude yield range for any possible two-photon absorption yield. Noticeable is a set of ''two-photon dark pulses'' inducing widely tunable three-photon absorption.

DOI: 10.1103/PhysRevLett.100.193002 PACS numbers: 32.80.Qk, 32.80.Wr, 42.65.Re

When a quantum system is irradiated with a broadband femtosecond pulse, a coherent manifold of quantum pathways is photo-induced from one state to the other. Shaping the pulse [1] to manipulate the interferences among these pathways is the means by which femtosecond coherent control affects state-to-state transition probabilities [2–7]. When several excitation channels to different final states of the system are of concern, in many cases it is sufficient to achieve basic multichannel selective control (on-off type) of maximizing one channel while minimizing the other channels. However, in other cases, a much higher degree of selectivity is desirable, where one channel is tuned independently over a wide yield range while the other channels are set constant on various chosen yields. This requires pulse shapes that reduce the correlations between the yields of the different channels.

Such extended multichannel selective femtosecond control has been experimentally studied so far mostly by employing automatic ''black-box'' optimization of the pulse shape using learning algorithms [8–13]. Here we focus on rational femtosecond coherent control, where the pulse shaping is based on identifying first the state-to-state interfering pathways and their interference mechanism. By itself rational femtosecond control is suitable mainly to quantum systems of limited complexity; however, it also provides a basis for control principles that are relevant for systems of high complexity. To date, the only rational femtosecond control work studied aspects of extended multichannel selective control is the one by Dudovich *et al.* [14] on polarization control of two-photon absorption to different angular-momentum states. All the other past studies of rational selective femtosecond control involve the simpler (on-off) scheme [15–18].

In this Letter, we introduce and demonstrate a new rational scheme for extended multichannel selective femtosecond coherent control that is based on symmetry properties of the excitation channels. The present processes are multiphoton absorption processes that generally are of fundamental and applicative importance and have been coherently controlled very effectively [7,14,16–30]. The current scenario involves a nonresonant two-photon absorption channel that is coherently incorporated in a resonance-mediated (2+1) three-photon absorption channel. The single-channel control over each of them has previously been studied separately [19,27]. Here, by utilizing a symmetry property of the two-photon channel for proper pulse shaping, the three-photon absorption is tuned independently over order-of-magnitude yield range for any possible yield of the two-photon absorption. The approach developed here is general, conceptually simple, and very effective.

Figure 1 shows the atomic dual-channel scheme considered here, involving an initial ground state $|g\rangle$ and two excited states $|f_1\rangle$ and $|f_2\rangle$. Irradiation with a weak (shaped) femtosecond pulse simultaneously induces a nonresonant two-photon absorption from $|g\rangle$ to $|f_1\rangle$ and a resonance-mediated (2+1) three-photon absorption from $|g\rangle$ to $|f_2\rangle$ with $|f_1\rangle$ as an intermediate state. The final

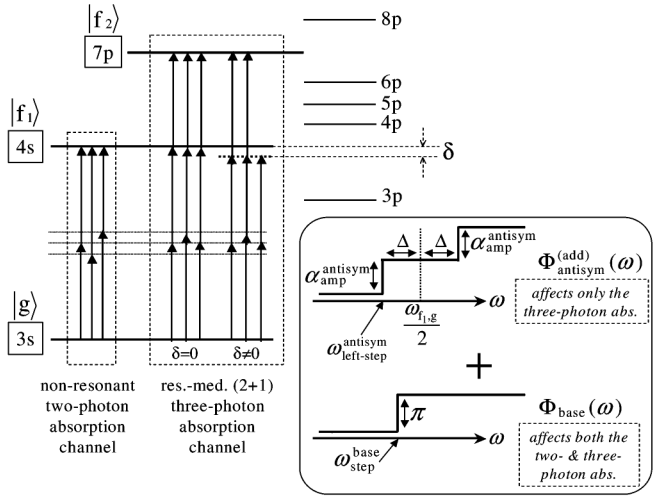

FIG. 1. The dual-channel femtosecond excitation scheme of Na. The inset schematically shows the base phase patterns and the antisymmetric phase additions used in the extended selective coherent control scheme.

amplitudes A_{f_1} and A_{f_2} of $|f_1\rangle$ and $|f_2\rangle$ after the pulse are given by [19,27]:

$$A_{f_1} = -\frac{1}{i\hbar^2}\mu_{f_1,g}^2 A^{(2)}(\omega_{f_1,g}), \quad (1)$$

$$A_{f_2} = \frac{1}{\hbar^3}\mu_{f_2,f_1}\mu_{f_1,g}^2[A_{f_2}^{(2+1)\text{on-res}} + A_{f_2}^{(2+1)\text{near-res}}], \quad (2)$$

$$A_{f_2}^{(2+1)\text{on-res}} = i\pi E(\omega_{f_2,f_1})A^{(2)}(\omega_{f_1,g}),$$

$$A_{f_2}^{(2+1)\text{near-res}} = -\wp\int_{-\infty}^{\infty}\frac{1}{\delta}A^{(2)}(\omega_{f_1,g}-\delta)E(\omega_{f_2,f_1}+\delta)d\delta,$$

with $A^{(2)}(\Omega) = \int_{-\infty}^{\infty} E(\omega)E(\Omega-\omega)d\omega$. The μ_{f_2,f_1} and $\mu_{f_1,g}^2$ are, respectively, the $|f_2\rangle - |f_1\rangle$ dipole matrix element and $|f_1\rangle - |g\rangle$ nonresonant two-photon coupling [19], and $\omega_{m,n}$ is the transition frequency between two states. $E(\omega) \equiv |E(\omega)|\exp[i\Phi(\omega)]$ is the pulse spectral field, with $|E(\omega)|$ and $\Phi(\omega)$ being, respectively, the spectral amplitude and phase of frequency ω. For the (unshaped) transform-limited (TL) pulse, $\Phi(\omega) = 0$. The final populations of $|f_1\rangle$ and $|f_2\rangle$ are $P_{f_1} = |A_{f_1}|^2$ and $P_{f_2} = |A_{f_2}|^2$. They serve, respectively, as the measures for the two- and three-photon absorption yields.

The above frequency-domain formulation allows us to identify the interfering pathways contributing to the final amplitudes (see Fig. 1): A_{f_1} interferes all the two-photon pathways from $|g\rangle$ to $|f_1\rangle$, while A_{f_2} interferes all the three-photon pathways from $|g\rangle$ to $|f_2\rangle$, each detuned by δ from $|f_1\rangle$. The on- ($\delta = 0$) and near-resonant ($\delta \neq 0$) pathways are interfered separately in $A_{f_2}^{(2+1)\text{on-res}}$ and $A_{f_2}^{(2+1)\text{near-res}}$ ($\wp$ is the Cauchy principal value). The different amplitudes are expressed using the parameterized $A^{(2)}(\Omega)$ interfering all the two-photon pathways of transition frequency Ω: A_{f_1} and $A_{f_2}^{(2+1)\text{on-res}}$ are proportional to $A^{(2)}(\omega_{f_1,g})$, while $A_{f_2}^{(2+1)\text{near-res}}$ integrates all $A^{(2)}(\omega_{f_1,g}-\delta)$ with $\delta \neq 0$.

In order to achieve a high degree of selectivity between the two- and three-photon absorption channels we utilize transformations $\hat{U}^{\text{selective}}$ of the spectral field $E(\omega)$ that do not change the two-photon absorption yield (P_{f_1}) but do change the three-photon absorption yield (P_{f_2}). This invariance of the two-photon channel is the symmetry property that we exploit. Based on Eqs. (1) and (2), it applies to any phase transformation $\hat{U}^{\text{selective}} = \exp[i\Phi_{\text{antisym}}^{(\text{add})}(\omega)]$ that keeps $|E(\omega)|$ unchanged while adding to $\Phi(\omega)$ a $\Phi_{\text{antisym}}^{(\text{add})}(\omega)$ that is antisymmetric around $\omega_{f_1,g}/2$, i.e.,

$$\Phi_{\text{antisym}}^{(\text{add})}(\omega_{f_1,g}/2+\beta) - \Phi_{\text{antisym}}^{(\text{add})}(\omega_{f_1,g}/2) = -[\Phi_{\text{antisym}}^{(\text{add})}(\omega_{f_1,g}/2-\beta) - \Phi_{\text{antisym}}^{(\text{add})}(\omega_{f_1,g}/2)]$$

for any value of β, with possibly different values of $\Phi_{\text{antisym}}^{(\text{add})}(\frac{\omega_{f_1,g}}{2}+|\beta|)$ for different values of $|\beta|$.

The effect of adding $\Phi_{\text{antisym}}^{(\text{add})}(\omega)$ to an existing $\Phi(\omega)$ can be explained as follows. Since a two-photon pathway from $|g\rangle$ to $|f_1\rangle$ is composed of a photon pair $\omega \equiv \frac{\omega_{f_1,g}}{2} - \beta$ and $\omega_{f_1,g} - \omega \equiv \frac{\omega_{f_1,g}}{2} + \beta$, it contributes to $A^{(2)}(\omega_{f_1,g})$ an amplitude of $|E(\frac{\omega_{f_1,g}}{2}-\beta)||E(\frac{\omega_{f_1,g}}{2}+\beta)| \times \exp\{i[\Phi(\frac{\omega_{f_1,g}}{2}-\beta)+\Phi(\frac{\omega_{f_1,g}}{2}+\beta)]\}$. So, adding $\Phi_{\text{antisym}}^{(\text{add})}(\omega)$ multiplies any such pathway amplitude by the same phase factor of $\exp[i2\Phi_{\text{antisym}}^{(\text{add})}(\frac{\omega_{f_1,g}}{2})]$. Consequently, the only effect on $A^{(2)}(\omega_{f_1,g})$ is its multiplication by this (global) phase factor and, thus, $|A_{f_1}|$ and P_{f_1} are kept unchanged. Conversely, since all the above does not apply to the pathways of $A^{(2)}(\omega_{f_1,g}-\delta)$ with $\delta \neq 0$, adding $\Phi_{\text{antisym}}^{(\text{add})}$ does alter $|A_{f_2}|$ and P_{f_2}.

Hence, the following extended selective coherent control scheme for designing the spectral phase pattern $\Phi(\omega)$ is applied: The two-photon absorption yield is set to a chosen value $P_{f_1,\text{base}}$ by choosing a proper base phase pattern $\Phi_{\text{base}}(\omega)$. Then, by adding different suitable antisymmetric phase patterns $\Phi_{\text{antisym}}^{(\text{add})}(\omega)$, the three-photon absorption yield is tuned from its base value $P_{f_2,\text{base}}$ over a wide range of values, while P_{f_1} is kept constant on $P_{f_1,\text{base}}$. The total phase pattern is $\Phi(\omega) = \Phi_{\text{base}}(\omega) + \Phi_{\text{antisym}}^{(\text{add})}(\omega)$. It is generally not antisymmetric around $\omega_{f_1,g}/2$.

The phase patterns chosen here as $\Phi_{\text{base}}(\omega)$ and $\Phi_{\text{antisym}}^{(\text{add})}(\omega)$ are shown schematically in Fig. 1. The present base patterns $\Phi_{\text{base}}(\omega)$ are of a single π step at variable position $\omega_{\text{step}}^{\text{base}}$. They allow a high degree of control over the full range of the nonresonant two-photon absorption [19]: from zero absorption, corresponding to "two-photon dark pulses", up to the maximal absorption when the interferences among all the two-photon pathways are fully constructive, as occurs with the TL pulse. They are also very effective in controlling the resonance-mediated (2+1) three-photon absorption [27]. Each of the present antisymmetric phase additions $\Phi_{\text{antisym}}^{(\text{add})}(\omega)$ is composed of two steps of equal amplitude $\alpha_{\text{amp}}^{\text{antisym}}$ in the range of $0-2\pi$. The steps are positioned symmetrically around $\omega_{f_1,g}/2$ at variable positions that are represented by the left-step position $\omega_{\text{left-step}}^{\text{antisym}}$. Since $|A_{f_1}|$ and $|A_{f_2}|$, and thus the absorption yields, are insensitive to a global phase of $E(\omega)$, for convenience, without loosing any generality, one can consider $\Phi_{\text{base}}(\frac{\omega_{f_1,g}}{2}) = 0$ and $\Phi_{\text{antisym}}^{(\text{add})}(\frac{\omega_{f_1,g}}{2}) = 0$.

The model system of the study is the sodium (Na) atom [31], with the $3s$ ground state as $|g\rangle$, the $4s$ state as $|f_1\rangle$, and the $7p$ state as $|f_2\rangle$ (see Fig. 1). The transition frequencies are $\omega_{f_1,g} \equiv \omega_{4s,3s} = 25740\ \text{cm}^{-1}$ (two 777-nm photons) and $\omega_{f_2,f_1} \equiv \omega_{7p,4s} = 12\,801\ \text{cm}^{-1}$ (one 781.2-nm photon). The $3s$-$4s$ two-photon coupling is nonresonant via the

p states. The Na interacts with phase-shaped linearly-polarized pulses with a Gaussian intensity spectrum centered at 780 nm with 5.8-nm bandwidth (~180-fs TL duration). The TL peak intensity is below 10^9 W/cm^2.

Experimentally, sodium vapor in a cell is irradiated with the laser pulses after they undergo shaping in a setup incorporating a pixelated liquid-crystal spatial light phase modulator [1]. The shaping resolution is 2.05 cm^{-1}. The population excited to the $4s$ state decays to the $3p$ state, which then decays to the $3s$ state. The $3p$-$3s$ fluorescence (at 589 nm) serves as the relative measure for the total $4s$ population $P_{f_1} \equiv P_{4s}$. The population excited to the $7p$ state undergoes radiative and collisional decay to lower excited states, including the $4d$, $5d$, $6d$, and $6s$ states. The fluorescence (at 460–570 nm range) emitted in their following decay to the $3p$ state serves as the relative measure for the total $7p$ population $P_{f_2} \equiv P_{7p}$. The emission is measured using a spectrometer coupled to a time-gated camera system, with a detection gate width of 25 and 1000 ns for P_{4s} and P_{7p}, respectively. As expected, the P_{4s} and P_{7p} exhibit, respectively, I^2 and I^3 dependence on the TL peak pulse intensity I.

Figure 2(a) presents experimental (squares and circles) and theoretical (lines) results for the basic phase control of the dual-channel absorption in Na using the base π-step patterns $\Phi_{\text{base}}(\omega)$. Shown are P_{4s} (squares and black line) and P_{7p} (circles and gray line) for the two- and three-photon absorption, respectively, as a function of the π-step position $\omega_{\text{step}}^{\text{base}}$. Each trace is normalized by the corresponding P_{4s} or P_{7p} excited by the TL pulse. The theoretical results are calculated numerically using Eqs. (1) and (2). As seen, there is an excellent agreement between the experimental and theoretical results. The nonresonant two-photon absorption is controlled from zero up to the TL absorption [19]. The zero absorption corresponds to the two dark pulses occurring when $\omega_{\text{step}}^{\text{base}} = 12\,896$ and $12\,844$ cm^{-1}. Its upper limit is measured here to be 300-fold smaller than the TL absorption, as set by the best-achieved experimental noise. The resonance-mediated (2+1) three-photon absorption is experimentally controlled from 3% to 240% of the TL absorption [27]. The strong enhancement occurs when $\omega_{\text{step}}^{\text{base}} = \omega_{7p,4s} = 12\,801$ cm^{-1}. It results from constructive interferences between positively ($\delta > 0$) and negatively detuned ($\delta < 0$) near-resonant $3s$-$7p$ three-photon pathways [27]. Overall, the π-step position simultaneously sets the two- and three-photon absorption yields to specific correlated values.

Implementing the symmetry-based selective control scheme presented above strongly reduces this correlation. Figures 3(a)–3(c) show several examples with different $\omega_{\text{step}}^{\text{base}}$ setting the two-photon absorption to the different levels ($P_{4s,\text{base}}$) indicated in the insets. The main graphs display the TL-normalized three-photon absorption (P_{7p}) resulting from different double-step antisymmetric phase additions $\Phi_{\text{antisym}}^{(\text{add})}(\omega)$ with $\alpha_{\text{amp}}^{\text{antisym}} = \pi$, as a function of the left π-step position $\omega_{\text{left-step},\pi}^{\text{antisym}}$. Shown are well-agreed experimental (circles) and theoretical (lines) results.

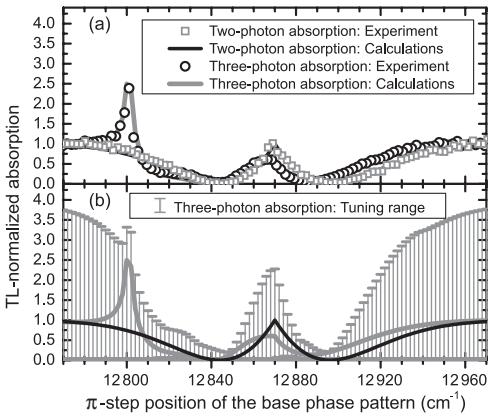

FIG. 2. (a) Experimental and calculated results for the basic femtosecond coherent control over the dual-channel absorption in Na using π-step patterns. (b) The complete picture of the corresponding symmetry-based selective coherent control. The lines are the basic control results of (a). The bars indicate the extended tuning range of the three-photon absorption for the different levels of the two-photon absorption.

Figure 3(a) shows the results for the case of zero two-photon absorption set by $\omega_{\text{step}}^{\text{base}} = 12\,896$ cm^{-1}. By scanning $\omega_{\text{left-step},\pi}^{\text{antisym}}$ across the spectrum, the three-photon absorption is continuously tuned experimentally from below 1% up to 20% of the TL absorption while the two-photon absorption is kept constant on its zero level. In other words, these results correspond to a family of shaped pulses that are all dark with respect to the two-photon absorption, while each of them induces a different three-photon absorption tunable over an order-of-magnitude yield range. The present tuning range is determined only by the component $A_{7p}^{(2+1)\text{near-res}}$ of the three-photon absorption amplitude A_{7p}, since a two-photon dark pulse ($A_{4s} = 0$) also leads to $A_{7p}^{(2+1)\text{on-res}} = 0$.

Figure 3(c) shows the results for the maximal (TL) two-photon absorption with $\omega_{\text{step}}^{\text{base}}$ outside the spectrum. By changing $\omega_{\text{left-step},\pi}^{\text{antisym}}$, the three-photon absorption is continuously tuned experimentally from 25% up to ~300% of the TL absorption while the two-photon absorption is kept maximal. The strong enhancement of the three-photon absorption occurs when $\omega_{\text{left-step},\pi}^{\text{antisym}} = \omega_{7p,4s}$. Also here, it is due to constructive interferences among near-resonant $3s$-$7p$ three-photon pathways [27].

Because of the finite experimental shaping resolution, the continuous theoretical tuning curve of the three-photon absorption in Fig. 3(c) is not fully probed experimentally around the enhancement position. However, most of this partially probed yield range is accessed experimentally by using another set of double-step antisymmetric phase additions, where $\omega_{\text{left-step}}^{\text{antisym}} = \omega_{7p,4s}$ and $\alpha_{\text{amp}}^{\text{antisym}}$ is scanned

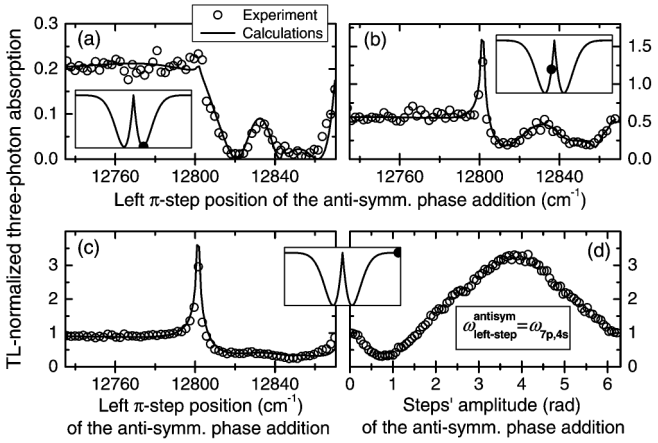

FIG. 3. Experimental and calculated results for examples of the symmetry-based selective control implementation. Each panel shows the three-photon absorption resulting from different antisymmetric double-step phase patterns added to a base π-step that sets the two-photon absorption to the level indicated in the inset: (a) zero, (b) intermediate, (c,d) maximal. The antisymmetric phase additions are of (a)–(c) $\{\alpha_{\mathrm{amp}}^{\mathrm{antisym}} = \pi$, variable $\omega_{\mathrm{left\text{-}step}}^{\mathrm{antisym}}\}$, (d) $\{\omega_{\mathrm{left\text{-}step}}^{\mathrm{antisym}} = \omega_{7p,4s}$, variable $\alpha_{\mathrm{amp}}^{\mathrm{antisym}}\}$.

from 0 to 2π. This is shown in Fig. 3(d), with a continuous tuning over 30%–330% of the TL absorption.

The complete picture for the extended selective control of the dual-channel absorption in Na is shown in Fig. 2(b), presenting numerical-theoretical results for the TL-normalized two- and three-photon absorption. Their base levels, set by a π-step at $\omega_{\mathrm{step}}^{\mathrm{base}}$, are shown by black and gray lines as in Fig. 2(a). The bar around each three-photon absorption point at $\omega_{\mathrm{step}}^{\mathrm{base}}$ indicates the extended tuning range of the three-photon absorption, achieved by applying all the possible double-step antisymmetric phase additions of any $\alpha_{\mathrm{amp}}^{\mathrm{antisym}}$ and any $\omega_{\mathrm{left\text{-}step}}^{\mathrm{antisym}}$, with the two-photon absorption kept constant on its corresponding base level. As seen, the three-photon absorption can be tuned independently over a wide yield range of more than an order of magnitude for any possible two-photon absorption yield. Hence, a high degree of independent selective control is achieved among the two absorption channels and their degree of correlation is considerably reduced as compared to using only the base π-step patterns. Quantitatively, the base levels of the two- and three-photon absorption as well as the tuning range of the three-photon absorption depend on the pulse spectral bandwidth. Still, qualitatively, a comparable degree of high selectivity among the two channels is achieved with any spectral bandwidth.

In conclusion, we have introduced and demonstrated a new scheme for achieving a high degree of selective femtosecond coherent control among multiple excitation channels. By proper pulse design, exploiting a symmetry property of one of the channels, the channel with the symmetry is set constant on a chosen possible yield while the other channels are tuned over a wide range of yields. When many channels are involved, the scheme can be applied iteratively to utilize different symmetry properties of different channels. Amplitude and polarization shaping [1] are natural extensions to the phase shaping employed here. Once corresponding symmetry properties are identified, the new scheme can be used in various multichannel scenarios, possibly involving also photoionization and dissociation.

This research was supported by The Israel Science Foundation (Grant No. 127/02) and by The James Franck Program in Laser Matter Interaction.

*amitayz@tx.technion.ac.il

[1] A. M. Weiner, Rev. Sci. Instrum. **71**, 1929 (2000); T. Brixner and G. Gerber, Opt. Lett. **26**, 557 (2001).
[2] D. J. Tannor, R. Kosloff, and S. A. Rice, J. Chem. Phys. **85**, 5805 (1986).
[3] M. Shapiro and P. Brumer, *Principles of the Quantum Control of Molecular Processes* (Wiley, NJ, 2003).
[4] W. S. Warren *et al.*, Science **259**, 1581 (1993).
[5] R. J. Gordon and S. A. Rice, Annu. Rev. Phys. Chem. **48**, 601 (1997).
[6] H. Rabitz *et al.*, Science **288**, 824 (2000).
[7] M. Dantus and V. V. Lozovoy, Chem. Rev. **104**, 1813 (2004); Chem. Phys. Chem. **6**, 1970 (2005).
[8] R. Judson and H. Rabitz, Phys. Rev. Lett. **68**, 1500 (1992).
[9] T. Brixner and G. Gerber, Chem. Phys. Chem. **4**, 418 (2003); P. Nuernberger *et al.*, Phys. Chem. Chem. Phys. **9**, 2470 (2007).
[10] T. C. Weinacht *et al.*, J. Phys. Chem. A **103**, 10 166 (1999).
[11] R. Levis, G. Menkir, and H. Rabitz, Science **292**, 709 (2001).
[12] J. Herek *et al.*, Nature (London) **417**, 533 (2002).
[13] D. Cardoza *et al.*, J. Chem. Phys. **122**, 124306 (2005).
[14] N. Dudovich, D. Oron, and Y. Silberberg, Phys. Rev. Lett. **92**, 103003 (2004).
[15] T. Baumert *et al.*, Phys. Rev. Lett. **67**, 3753 (1991).
[16] A. M. Weiner *et al.*, Science **247**, 1317 (1990).
[17] N. Dudovich *et al.*, Nature (London) **418**, 512 (2002).
[18] M. Wollenhaupt *et al.*, Phys. Rev. A **68**, 015401 (2003).
[19] D. Meshulach and Y. Silberberg, Nature (London) **396**, 239 (1998); Phys. Rev. A **60**, 1287 (1999).
[20] A. Präkelt *et al.*, Phys. Rev. A **70**, 063407 (2004).
[21] N. Dudovich *et al.*, Phys. Rev. Lett. **86**, 47 (2001).
[22] B. Chatel *et al.*, Phys. Rev. A **70**, 053414 (2004).
[23] P. Panek and A. Becker, Phys. Rev. A **74**, 023408 (2006).
[24] E. Gershgoren *et al.*, Opt. Lett. **28**, 361 (2003).
[25] H. U. Stauffer *et al.*, J. Chem. Phys. **116**, 946 (2002); J. B. Ballard *et al.*, *ibid.* **116**, 1350 (2002).
[26] S. Lim *et al.*, Phys. Rev. A **72**, 041803 (2005).
[27] A. Gandman *et al.*, Phys. Rev. A **75**, 031401(R) (2007); **76**, 053419 (2007).
[28] L. Chuntonov *et al.*, J. Phys. B **41**, 035504 (2008); Phys. Rev. A **77**, 021403(R) (2008).
[29] N. Dudovich *et al.*, Phys. Rev. Lett. **94**, 083002 (2005).
[30] C. Trallero-Herrero *et al.*, Phys. Rev. Lett. **96**, 063603 (2006).
[31] NIST Atomic Spectra Database (NIST, Gaithersburg, MD, 2007).